

10. COD and Stretched Zone as the Criterion for Fracture Initiation from a Precrack at Various Temperatures

Akio OTSUKA*, *Member*, Takashi MIYATA*, *Member*,
Seiji NISHIMURA*, *Member*, Makoto OHASHI**,
Yoichiro KASHIWAGI**

(From *J.S.N.A. Japan*, Vol. 135, June 1974; Vol. 136, Dec. 1974)

Summary

This paper consists of part I and part II.

In part I, "Fracture Initiation from a Precrack and COD-Criterion", the effects of plastic constraint and temperatures on fracture initiation from a notch were investigated by using various types of notched specimens, at the temperatures ranging from room temperature to liquid nitrogen temperature.

The results show that, when fracture initiates by fibrous crack, the COD at fibrous crack initiation is almost independent of plastic constraint of the specimens or of the test temperatures, while the COD at maximum load or at final fracture is largely dependent on them. When fracture initiates by cleavage crack, the critical COD also shows considerable dependence on those parameters above mentioned. These behaviors of critical COD are explained by the fracture mechanism in each mode of fracture.

In part II, "COD-Criterion and Stretched Zone", the behavior of the stretched zone and fracture initiation at the notch root with increase of the applied load has been investigated at various temperatures.

The stretched zone width is almost constant regardless of test temperatures when crack initiates by fibrous crack, while, in the case of cleavage initiation, it takes various values between the above-mentioned value and zero depending on temperature and plastic constraint.

When fracture occurs with plastic COD, the critical COD at fracture is reduced by the amount of stretched zone given by the preloading, while the effect of preloading on the critical COD is small when the COD mainly consists of elastic deformation.

The process of fracture initiation from the tip of 45° crack has also been investigated and it is found that the stretched zone width of 45° crack specimen is about the same as that in mode I.

Part I. Fracture Initiation from a Precrack and COD Criterion

I.1 Introduction

Although the effectiveness and the validity of the COD-criterion, as the design concept which is based on the prevention of failure,

have already been confirmed in many respects,^{1~4)} there are still some problems left before this concept can be used in practical applications.

One problem arises from the fact that a critical COD value is not a material constant in the strict sense but rather a variable depending on mechanical factors, such as specimen geometry and strain rates and so on. Another problem arises from the fact

* Department of Iron and Steel Engineering, Nagoya University

** Kawasaki Steel Corp.

that the analytical expression of COD as a function of defect size and applied load has not been obtained in the general yield region in which the COD concept will be the most appropriate fracture criterion.

Part I relates to the former problems where some experimental investigations were made on the effects of plastic constraint around the crack tip as well as the validity and the limitation of the COD criterion with relation to the fracture mechanism.

I.2 Materials, Specimens and Experimental Details.

Chemical compositions and mechanical properties of the five steels used in this investigation are shown in Table 1 and 2, respectively.

Steel C is the 50 kg/mm² class steel (JIS SM50C) and all the other steels are mild steel (JIS SS41). Steels A, C, D, and E are rolled plates of 22 mm thick, 25 mm thick, 12 mm thick and 3 mm thick, respectively. Steel B is a 60 mm diameter round bar.

The following four series of experimental

investigations were conducted:

a) Effect of plastic constraint on the critical COD value was investigated in center-notched tension plates of various thickness, side-grooved tension plates and circumferentially-

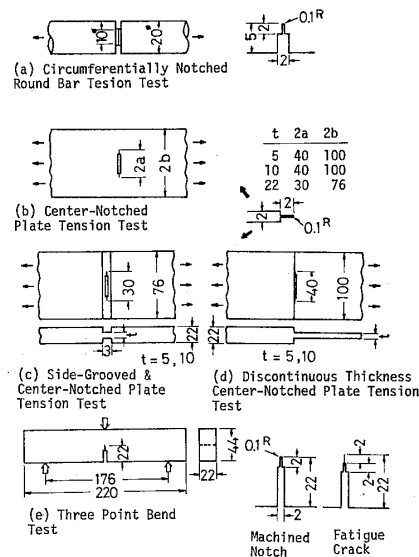


Fig. 1 Test specimens for Steel-A, dimensions in mm

Table 1 Chemical Compositions (%)

Steel	C	Si	Mn	P	S
A(JIS-SS41), 22 mm thick plate	0.118	0.22	0.39	0.011	0.030
B(JIS-SS41), 60 mm dia. Round Bar	0.21	0.25	0.47	0.013	0.028
C(JIS-SM50C), 25 mm thick plate	0.16	0.30	1.40	0.013	0.013
D(JIS-SS41), 12 mm "	0.176	0.34	0.67	0.008	0.021
E(JIS-SS41), 3 mm "	0.18	0.006	0.52	0.028	0.017

Table 2 Mechanical properties and V-Charpy impact test results

Steel	Mechanical Properties				V-Charpy Test
	Yield Strength kg/mm ²	Tensile Strength kg/mm ²	Elongation %	Reduction of Area %	$vT_{rs}(^{\circ}C)$
Steel-A	26.7	43.9	23.0	67.0	+12
Steel-B	27.0	47.4	32.0	57.2	+29
Steel-C	34.7	52.2	32.7	71.9	-38
Steel-D	26.0	39.8	42.4	—	+ 5
Steel-E	29.9	42.7	42.3	—	—

notched round bars. Specimen details are shown in Fig. 1 and Steel A was used.

b) Circumferentially-notched round bars with different ratios of notch depth to specimen diameter were tested for investigating the effect of notch depth on the plastic constraint. Specimen details are shown in Fig. 2 and Steel B was used in this series of tests.

c) As a standard test on the Steels A and C, three-point notched bend tests were made with specimens shown in Figs. 1 and 3.

d) Effect of notch acuity was studied by testing circumferentially-notched round bar specimens with different notch root radius. Specimen details are shown in Fig. 3 and Steel C was used in this series of tests.

COD values were measured by using a clip gage in all tests.

The COD values measured by clip gages were converted to the notch tip values by using calculation obtained by finite element method, for all types of the specimens other than the slow bend tests.

Better agreements were obtained between the measured COD and the calculated COD

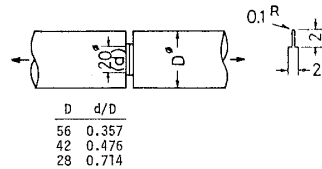


Fig. 2 Test specimens for Steel-B, dimensions in mm

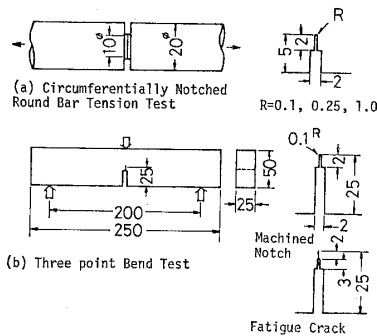


Fig. 3 Test specimens for Steel-C, dimensions in mm

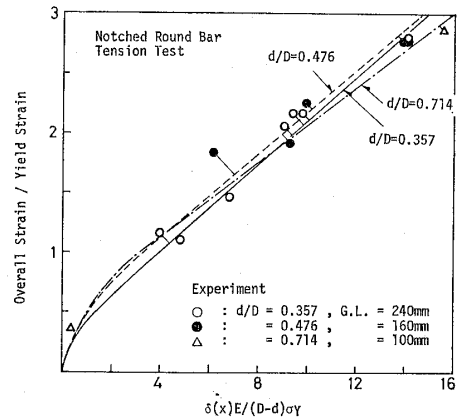


Fig. 4 Comparison between measured COD and COD calculated by FEM, Steel-B

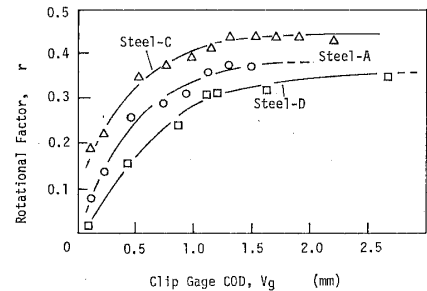


Fig. 5 Variation of rotational factor with clip gage COD for bend test

by FEM when comparison was made at the same specimen elongation than at the same load. Some examples of the Comparison at the same specimen elongation are shown in Fig. 4.

In slow bend tests, the notch tip COD for a range of low stress level was calculated from the fracture load using the FEM results by T. Kanazawa et al.⁴⁾ For the range of high stress level, the notch tip COD was calculated from the clip gage COD measured at notch end using the rotational factor, r . The values of measured rotational factor r are shown in Fig. 5 as the function of clip gage COD. Although Fig. 5 shows the values for 0.1 mm mechanical-notched specimens, the same values were used for fatigue-cracked specimens. The notch tip COD is given by the following equation,

$$\delta = \frac{Vg}{1 + (z+a)/r(d-a)} \quad (1)$$

where δ =notch tip COD, Vg =clip gage COD, d =specimen depth, a =notch depth and z =the distance above the specimen surface at which the measurement is made. The notch tip COD values obtained by this method agreed

well with those obtained by using the Wells' formula⁵⁾ in a wide range of stress levels.

The COD values at fibrous crack initiation, δ_i , were obtained by the off-load method described later.

1.3 Results and Discussion

(1) COD at maximum load

Critical COD, δ_c , at the maximum load of

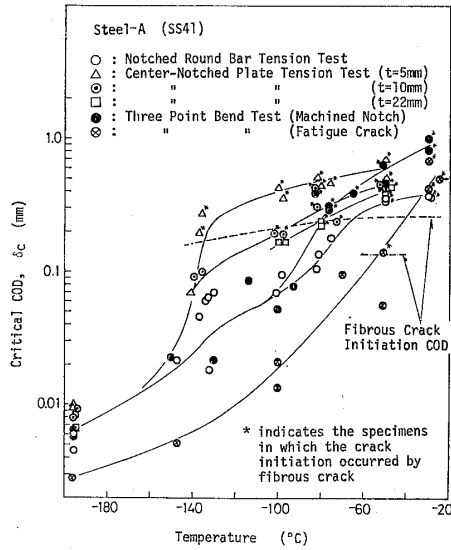


Fig. 6 Variation of critical COD with temperature, Steel-A

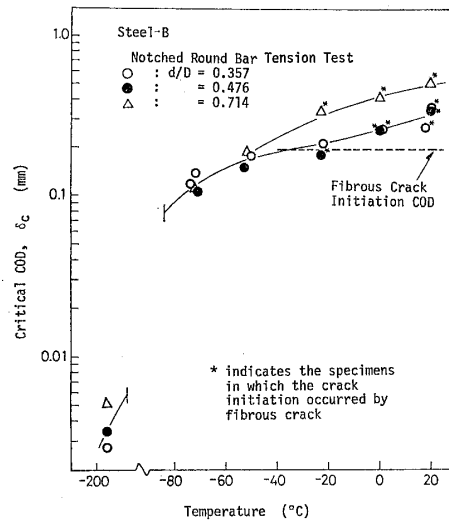


Fig. 8 Variation of critical COD with temperature, Steel-B

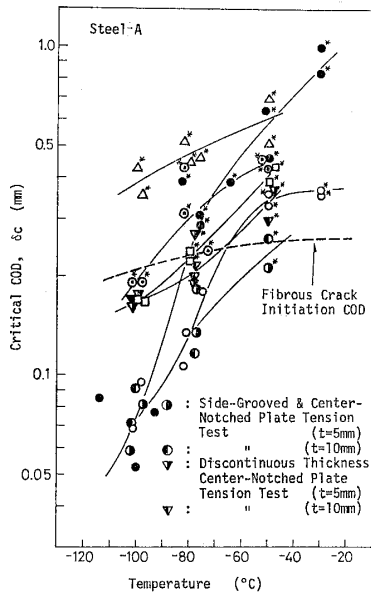


Fig. 7 Variation of critical COD with temperature, Steel-A

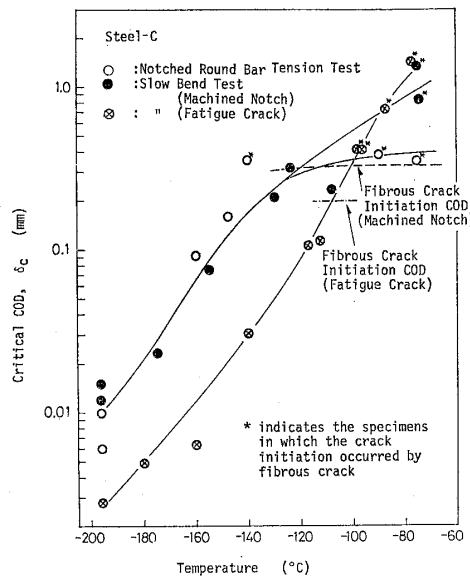


Fig. 9 Variation of critical COD with temperature, Steel-C

Steel A is shown in Figs. 6 and 7, and those of Steels B and C are shown in Figs. 8 and 9 respectively.

Unstable brittle fracture initiation occurred at the maximum load regardless of the steel tested, with the exception of the circumferentially-notched round bar tested in the high temperature region.

Critical COD values used in the present study are the values at the original notch tip position, in other words, the subcritical crack growth before unstable growth is not considered in converting the measured clip gage COD to "notch tip" value.

From Figs. 6 and 7, it is obvious that critical COD at maximum load, δ_c , takes widely different values according to the specimen geometry, as already shown by Terry⁶⁾ and Fearnough.⁷⁾ The dependence of δ_c on specimen geometry will be explained by the plastic constraint around the notch tip of the specimens as will be shown later in 1.3 (3).

To show the intensity of plastic constraint accurately, a three-dimensional analysis will be necessary. Figure 10 shows some examples of the relation between critical COD, δ_c , and

the ratio of general yield stress to uniaxial yield stress which expresses indirectly the intensity of the plastic constraint. It is seen that δ_c decreases with increasing plastic constraint (σ_{GY}/σ_Y).

(2) COD at Fibrous Crack Initiation

It is reported that COD at the instant of fibrous crack initiation, δ_i , takes almost a constant value, regardless of specimen geometry such as specimen width,^{6,7)} specimen thickness,⁸⁾ and the ratio of notch depth to specimen depth,⁶⁾ while the COD at maximum load varies with these parameters. Also S. Kanazawa et al.⁹⁾ recently reported that δ_i is not affected even by strain rate and test temperatures. If δ_i can be proven to be a general characteristic parameter or if conditions for its existence can be determined, δ_i will be a very good fracture criterion from the points of view of design application and study of fracture mechanism.

In this report, the values of δ_i were obtained by off-load method, which is explained later, at various temperatures on circumferentially-notched round bar and bend specimens of Steels A and C, and circumferentially-notched round bar of Steel B with three different

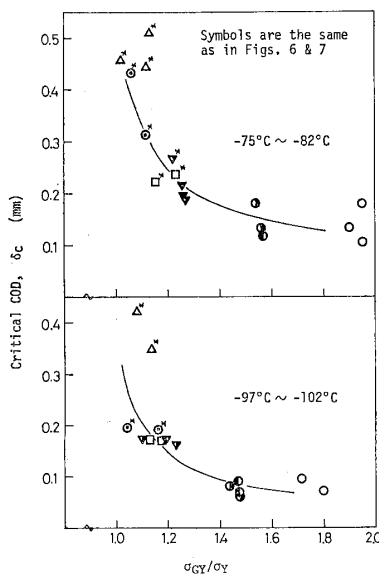


Fig. 10 Relation between critical COD and general yield stress of the various types of specimens

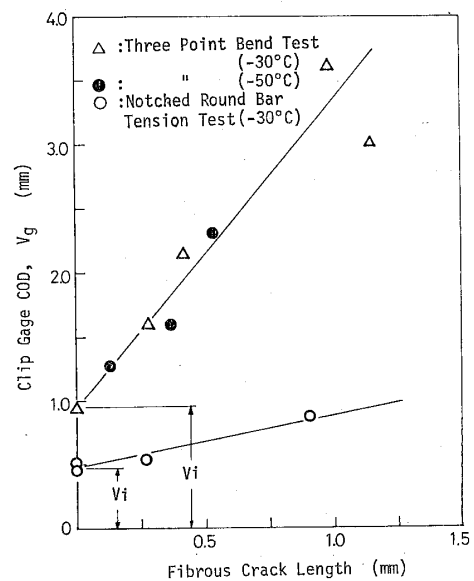


Fig. 11 Clip gage COD versus fibrous crack length, Steel-A

values of δ_i is as follows: specimens were off-notch depths. The method used to obtain the loaded during loading, broken in liquid nitrogen, and the fibrous crack lengths on the fracture surfaces were measured by Profile projector. By plotting the data, as shown in Fig. 11 and by extrapolating the curves to zero fibrous crack length, we obtained the values of COD for zero crack length. This value thus obtained is used as δ_i in this report. The values of δ_i of Steels A, B and C are shown in Fig. 12. Plots of COD at fibrous-cleavage transition are also included in these figures. These values are obtained by plotting the values of δ_e for each fibrous crack length from the data obtained at various test temperatures and extrapolating the δ_e vs. fibrous crack length curve obtained from the above plot (Fig. 13). The COD value at the

intersecting point, namely the point of zero fibrous crack length, represents the COD value at fibrous-cleavage transition. This value is δ_i at the lowest temperature where fibrous crack occurs, but it may also be used as a representative value of δ_i for this material since δ_i hardly varies with temperature as mentioned before. This method will be referred to as the "transition point method" since the other method was described as the "off-load method".

What is most remarkable in Fig. 12 is that δ_i of different specimens shows about the same value regardless of specimen geometries and that only a slight increase with increase in test temperature is noted as long as the temperature is in the fibrous crack initiation region. This characteristic of δ_i that it is almost independent of specimen geometry and temperature is very desirable property as a criterion for design which is based on fracture initiation. This design principle which is based on δ_i is also desirable from the view of safety of structures because this design principle means the prevention of fracture initiation. The temperature T_i , at which the transition from fibrous to cleavage in fracture initiation occurs, will be another important parameter along with δ_i . T_i varies largely according to the degree of plastic constraint as will be seen in Fig. 6. Then, an important problem is what value should be taken as T_i for the actual structures. Because δ_i is a value which represents ductility and T_i is a

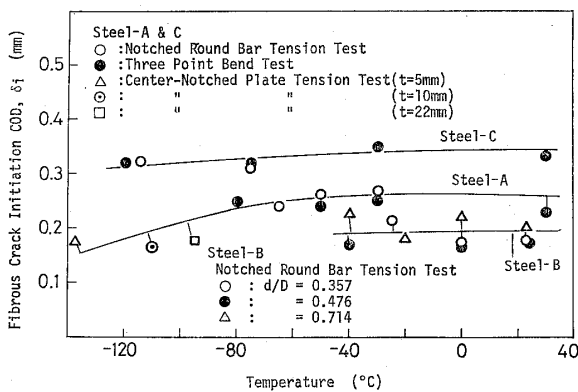


Fig. 12 Variation of fibrous crack initiation COD with temperature

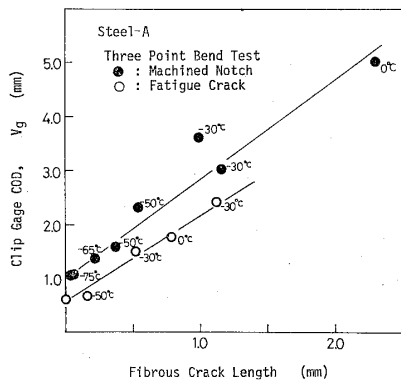


Fig. 13 Clip gage COD versus fibrous crack length at various temperatures

Table 3 Comparison between the results obtained by COD test (δ_i and T_i) and those by conventional test (reduction of area and Charpy transition temperature)

Steel	δ_i^* (at T_i , mm)	T_i^{**} (°C)	R.A. (%)	vT_{rs} (°C)	vT_r 5% (°C)
Steel-A	0.24	- 65	67.0	+12	-38
Steel-B	0.17	- 40	57.2	+29	-15
Steel-C	0.32	-114	71.9	-39	-74

* δ_i : Notch tip COD at fibrous crack initiation

** T_i : The lowest temperature at which crack initiation occurs by fibrous crack

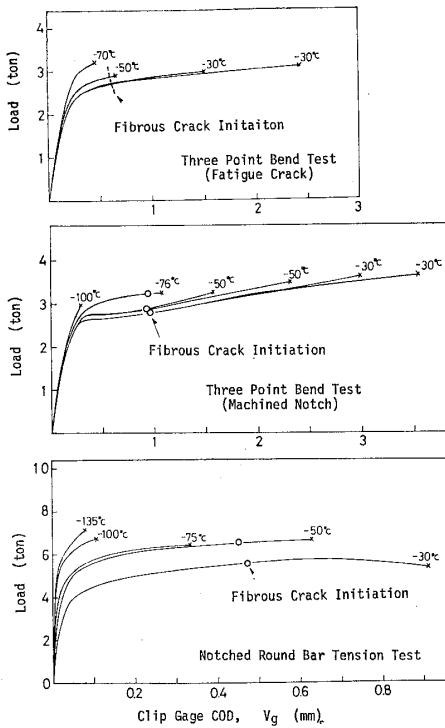


Fig. 14 Load-COD curve and fibrous crack initiation, Steel-A

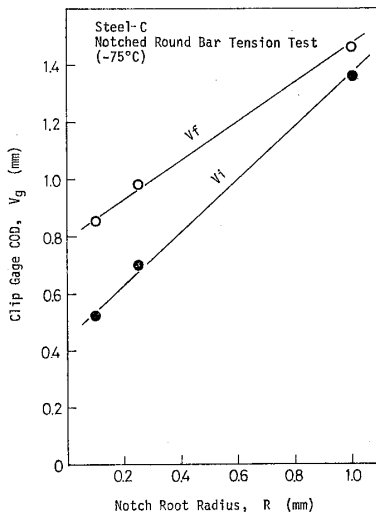


Fig. 15 Effects of notch root radius on clip gage COD

ductile-cleavage transition temperature, the comparison of these values with reduction of area obtained from usual tensile tests and Charpy transition temperature is made in Table 3. It is seen that some qualitative agreement

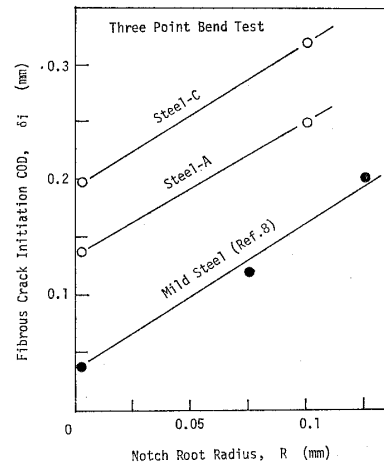


Fig. 16 Effects of notch root radius on fibrous crack initiation COD

is observed between the evaluation of toughness by δ_i and T_i and that by reduction of area and Charpy transition temperature.

Figure 14 shows some examples of clip gage COD~Load relation curves. It will be noticed that fibrous crack initiation occurs in relatively early stage of loading. Figures 15 and 16 show the effects of notch root radius on clip gage COD and fibrous crack initiation COD, respectively. It is seen in these figures that both clip gage COD and δ_i vary linearly with notch root radius. Although the data by Smith and Knott⁸⁾ show that COD at fibrous crack initiation is proportional to the slot width (COD is zero when slot width is zero), the present results that finite amount of δ_i are observed even in the case of fracture initiation from fatigue precrack seem to be more reasonable, because the stretched zone is always observed at the notch tip before fibrous crack initiation.

(3) Critical COD and Fracture Condition

Fracture mode transition has a significant effect, as Barsom and Rolfe¹⁰⁾ pointed out on the fracture toughness of medium strength steel and low strength steel. Fracture condition and critical COD at various temperatures will thus be discussed with particular attention to fracture mode.

Figure 17 is a schematic illustration of the relation between critical COD and fracture

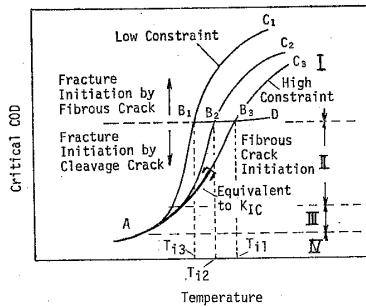


Fig. 17 Schematic relations between COD and fracture mode transition

mode. Because a detailed study of fracture behavior at various temperatures is given for smooth round bars by Hahn et al.,¹¹⁾ the analyses of the present results described in (1) and (2) are made in reference to their results.

Fracture initiation mode is divided by line BD; above this line or at higher temperature than T_i fracture occurs by fibrous type crack, and by cleavage below this line or at lower temperature than T_i . In the temperature region higher than T_i fibrous crack occurs when COD reaches the value BD and unstable fracture occurs at the curve BC. For low constraint and high temperature, unstable fracture could occur in fibrous or shear type, but usually in notched low strength steel specimens the initiation of unstable fracture coincides with the transition from fibrous crack growth to cleavage crack propagation. The former and the latter cases are named regions A and B, respectively by Hahn et al., and we call both regions region I as shown in Fig. 17. It has already been shown that the fibrous initiation curve BD shows little dependence on temperature and specimen geometry.

It is well known that fibrous crack occurs by void coalescence. McClintock¹²⁾ showed, at least in principle, that void growth is enhanced by both shearing stress and hydrostatic tension. However, the present experimental results which showed that δ_i has little dependence on specimen geometry in spite of the variation in plastic constraint, seem to imply that hydrostatic tension has

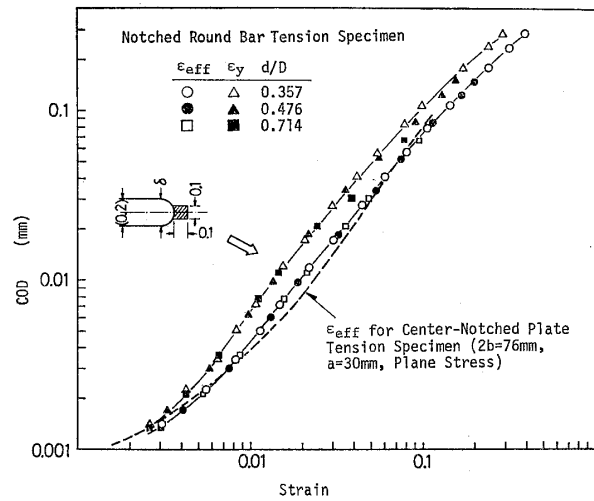


Fig. 18 Relation between COD and strain at notch tip calculated by FEM

little influence on fibrous crack initiation at the notch tip, as long as the variation of the hydrostatic tension is in the degree that is induced by the variation of the specimen geometry given in the present test.

In Fig. 18, comparison is made between the strain at the notch tip and COD. Although it is usual to take tensile strain ϵ_y as the strain which corresponds to COD, the effective strain $\epsilon_{eff} (= \sqrt{2}/3[(\epsilon_1 - \epsilon_2)^2 + (\epsilon_2 - \epsilon_3)^2 + (\epsilon_3 - \epsilon_1)^2]^{1/2}$, where ϵ_1 , ϵ_2 and ϵ_3 are the principal strains) around the notch tip (region of 0.1 mm \times 0.1 mm as shown in Fig. 18) was taken. It is shown in this figure that the relation between COD and ϵ_y COD and ϵ_{eff} for notched-round-bar tension specimen, and it is also noticed that the COD $\sim \epsilon_{eff}$ relation for notched-plate tension specimen is very similar to the one for notched-round-bar tension specimen. These facts seem to imply that the behavior of COD is the reflection of that of ϵ_{eff} (or τ_{eff}). Furthermore, it will be reasonable to consider that COD-criterion physically implies ϵ_{eff} -criterion for fibrous fracture initiation and τ_{eff} -criterion for cleavage fracture initiation. Further consideration will be made relating to the condition of fracture initiation in the following discussion.

In the intermediate temperature region, region II and III, fracture occurs by cleavage

Crack with considerable amount of COD. These regions, where cleavage occurs after plastic deformation, correspond to Hahn's regions C and D. These regions are characterized, as already mentioned in (1), by the large dependence of δ_c on specimen geometry (or plastic constraint of the specimen). Hahn et al. also reported that many micro-cracks are observed in regions C and D, and thus the theory by T. Yokobori¹³⁾ appears appropriate to explain this case. Yokobori considers the propagation of micro-crack in one grain by traversing the grain boundary as the critical event in fracture in this temperature region. The condition of the fracture is given by

$$A\sigma + B(\tau - \tau_i) = R \quad (2)$$

where A , B and R are the constants which depend on the material and geometry of the specimen.

In the lower temperature part of region III, however, the mechanism given by Stroh¹⁴⁾ and Cottrell¹⁵⁾, in which the critical stage is considered to be initial growth of the first micro-crack, seems to be more appropriate. The fracture condition is given as

$$\sigma(\tau - \tau_i) = C \quad (3)$$

where τ_i =frictional stress, C =material constant. In eqs. (2) and (3), σ and τ is the local tensile and shearing stresses in the element at the notch root induced by applied load. The most interesting fact in the above discussion is that fracture condition involves both σ and τ , whether the fracture condition is given by eq. (2) or by (3). This means that if the ratio of σ/τ in the element at the notch root varies, the values of τ and σ at fracture must also vary. In other words, the larger the constraint (the larger σ/τ), the smaller the τ at fracture. This explains the present results related to the effects of constraint on δ_c in that the larger the constraint, the smaller δ_c becomes since COD is determined by the amount of plastic deformation at the notch root. If the condition of fracture is further clarified together with the critical parameters, the estimation of δ_c for a given constraint will be possible.

In the region of relatively low temperature and high constraint, Fig. 6 shows that COD at fracture approaches some limiting value which depends on temperature. In the region where the value of COD attains this limiting value, the condition of plane strain is satisfied and thus this limiting value, as shown in Fig. 17, would correspond to K_{IC} . K_{IC} approach would thus be preferable to COD approach in such a region.

The fracture condition in region IV is considered to be τ =constant because this region corresponds to Hahn's region E where fracture occurs at the instant of initiation of yielding. In this region, the COD at fracture takes an almost constant value regardless of specimen geometry and temperature.

I.4 Conclusions

Condition of fracture initiation from a notch was investigated using low strength steels with particular attention to the fracture after large scale yielding.

Main conclusions are as follows:

a) The present results show that COD at fibrous crack initiation, δ_i , is a very important and effective criterion of ductile fracture initiation, due to its early initiation and little dependence on temperature and specimen geometry. From the practical view point, the value of δ_i can be obtained easily, without any special technique, from the data of conventional fracture tests at various temperatures by adding only the measurement of COD.

b) When fracture initiates as cleavage cracks after plastic straining, the value of COD at fracture shows a large variation depending on the degree of plastic constraint and temperature. Therefore, great care is required in evaluating crack-like defects in such a region,

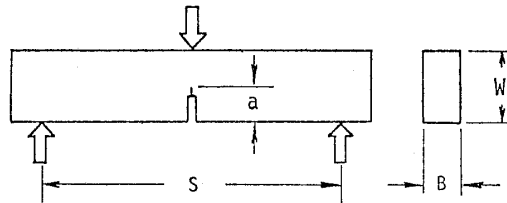
Part II. COD-Criterion and Stretched Zone

II.1 Introduction

It is already pointed out by several authors^{6,7,8,16)} that COD at the fibrous or ductile crack initiation, not at the maximum

Table 4 Dimensions of three point bend specimens, in mm

Steel	S	B	W	a	Notch Tip
Steel-A	176	22	44	22	Fatigue-precrack, 0.1 R
Steel-C	200	25	50	25	Fatigue-precrack, 0.1 R
Steel-D	120	12	30	15	Fatigue-precrack, 0.05 R, 0.1 R



load or unstable fracture, is a very effective criterion for fracture initiation from a sharp notch. Some ambiguities, however, still seem to exist concerning the behavior of the "crack tip COD" during the fracture process.

In the present study, the deformation behavior of the notch tip under the increasing load until fracture was investigated by microscopic observations by SEM.

The stretched zone observed at the fatigue precrack tip of fractured specimen, firstly noticed by Spitzig¹⁷⁾, is considered to be an important parameter which represents the behavior of the precrack tip of the specimen subjected to increasing load leading to fracture¹⁸⁻²¹⁾. In part II, the development of the stretched zone at the notch tip with increase of COD due to load increase was investigated at various temperatures with special attention to fibrous and cleavage crack initiation. The effects of preloading on the behavior of stretched zone at the crack initiation were also investigated. Some preliminary tests on the stretched zone in mixed mode conditions were also made.

II.2 Materials and Experiments

Chemical compositions and mechanical properties of steels used in the experiments are shown in Tables 1 and 2, respectively. Three point bend specimens are mainly used in order to investigate the deformation behavior of the notch tip under increasing load. The dimensions of the specimens used for

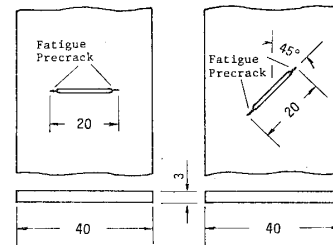


Fig. 19 90° and 45° Fatigue-precracked specimen, Steel-E, dimensions in mm

this purpose are shown in Table 4. In order to investigate the effects of the loading mode on stretched zone, 45° oblique fatigue-precracked specimens and 90° fatigue-precracked specimens shown in Fig. 19 were used. Measurements of the stretched zone width were made by SEM. The tilt angle for Mode I specimens were 45°, and for 45° oblique cracked specimens, the tilt angle were chosen in which the stretched zone width appears to be the largest. This angle was about 30°.

II.3 Results and Discussion

(1) Stretched Zone and Fibrous Crack Formation at the Notch Tip with Increase of COD under Increasing Load

The stretched zone formation with increase of applied load was investigated by fracturing the specimens in liquid nitrogen after off-loading at various loads before fracture. An example of the stretched region of Steel D is shown in Fig. 20. The COD was measured by clip gages attached at the end of the slit.

In Fig. 21, the results of fatigue-precracked

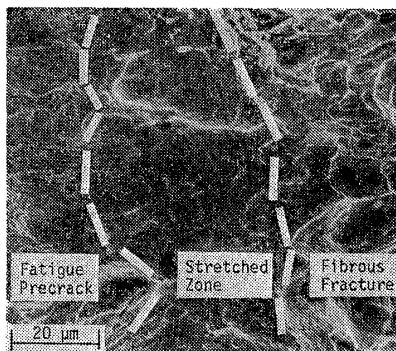


Fig. 20 Stretched zone of fatigue precracked bend specimen, Steel-D

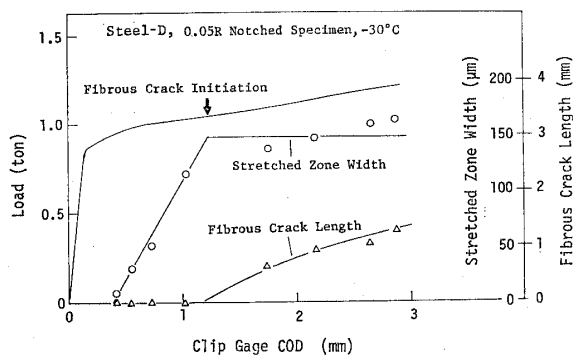


Fig. 22 Variation of load, stretched zone width and fibrous crack length with clip gage COD, Steel-D, 0.05 R-notched specimen, three point bend test

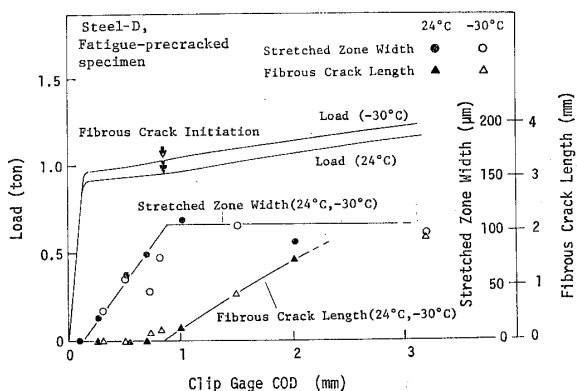


Fig. 21 Variation of load, stretched zone width and fibrous crack length with clip gage COD, Steel-D, fatigue-precracked specimen, three point bend test

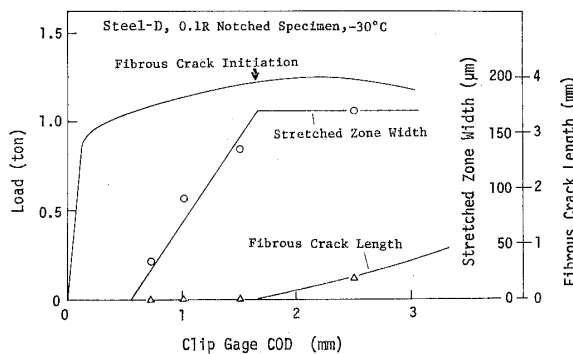


Fig. 23 Variation of load, stretched zone width and fibrous crack length with clip gage COD, Steel-D, 0.1 R-notched specimen, three point bend test

specimens, the data obtained from the tests at 24°C and -30°C are plotted. It is seen in this figure that the stretched zone is formed when COD attains to a certain value, and the size of the stretched zone increases with increase of COD until the size reaches a critical value at which fibrous crack initiates. After the initiation of fibrous crack, the size of the stretched zone does not change.

It is also interesting to notice that the relations between the stretched zone width and COD are independent of temperature, and that their values at fibrous crack initiation are almost independent of temperature, too.

The results of the mechanical-notched specimens shown in Figs. 22 and 23 show the similar situation to those of fatigue-precracked specimens shown in Fig. 21. In the case of

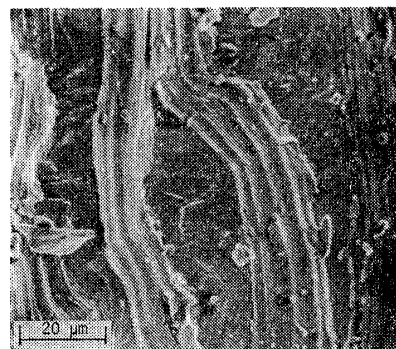


Fig. 24 Stretched zone of mechanical notched specimen, notch tip radius is 0.1 mm

mechanical-notched specimens, it will be noticed, however, that the critical sizes of the stretched zones for fibrous crack initiation and the value of the COD at which stretched

zone initiates at the notch root are a little larger than in the case of fatigue-precracked specimens. The stretched zone in mechanical-notched specimens is usually divided into several somewhat irregular bands by initially machined notch surface as shown in Fig. 24. In such a case, the sum of the width of the individual bands is used for the stretched zone width.

(2) *Stretched Zone Width and Fibrous Crack Length at Various Temperatures*

Because the stretched zone width does not alter after the crack initiation as stated in the previous section, the stretched zone width at the instant of fracture initiation can be

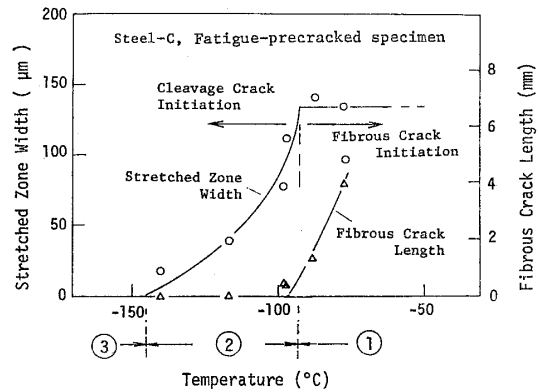


Fig. 27 Variation of stretched zone width and fibrous crack length with temperature, Steel-C, fatigue-precracked specimen, three point bend test

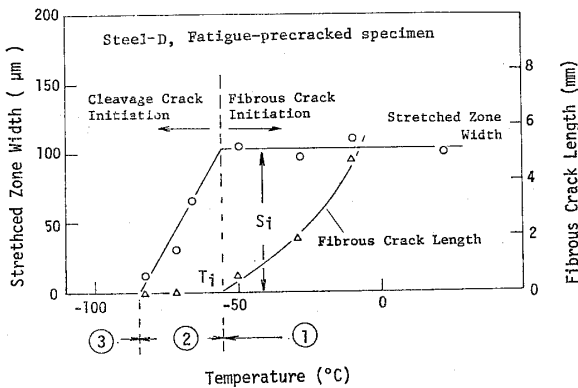


Fig. 25 Variation of stretched zone width and fibrous crack length with temperature, Steel-D, fatigue-precracked specimen, three point bend test

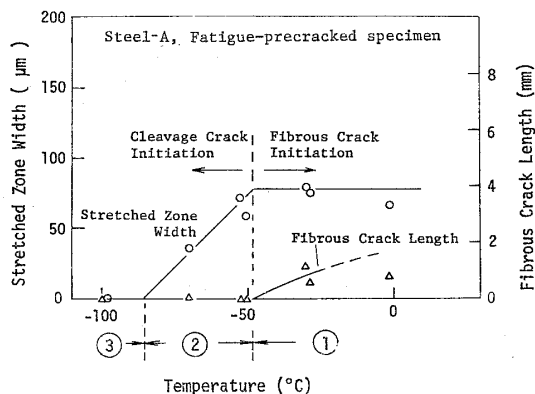


Fig. 26 Variation of stretched zone width and fibrous crack length with temperature, Steel-A, fatigue-precracked specimen, three point bend test

measured on the fracture surface after the fracture tests. The stretched zone width at the fracture initiation obtained by this method at various temperatures are shown in Figs. 25, 26 and 27, for Steels D, A and C, respectively.

It is seen that the notch tip behavior until fracture initiation is divided into three regions according to test temperatures, as shown in these figures.

In the region 1 fracture occurs by fibrous crack with stretched zone; in the region 2 fracture occurs by cleavage with stretched zone; and in the region 3 fracture occurs by cleavage without stretched zone.

It is evident from these figures that in the region 1 the S.Z.W. is almost constant regardless of test temperatures and almost zero in the region 3, while in the region 2 it takes various values between the value in the region 1 and zero.

In other words, the sizes of the stretched zone followed by fibrous crack (denoted by S_i in Fig. 25) are almost constant regardless of test temperatures, although those of the S.Z. followed by cleavage crack vary largely with test temperatures. It should also be noticed that the stretched zone width of this case is affected not only by temperature but also by plastic constraint, because the temperature of the fibrous-cleavage transition in fracture

initiation depends on plastic constraint.

The results on Steels A and C shown in Figs. 26 and 27, respectively, show the similar situations to the case of the Steel D shown before. Some differences, however, are observed in the temperatures of the fibrous-cleavage transition at the crack initiation (T_i) and in the amounts of S.Z.W. at which fibrous crack initiation occurs. The T_i of the Steels A and C are -50°C and -98°C respectively. The S.Z.W. of these steels are shown in Fig. 28.

(3) The Stretched Zone Width and COD at Fibrous Crack Initiation

The relation between COD obtained from S.Z.W. and that from clip gage COD at various notch acuity is shown in Fig. 28. Stretched zone width was converted to notch tip COD by multiplying $\sqrt{2}$. To convert the clip gage COD into the notch tip value, the rotational factor shown in eq. (1) in part I was used. The value of the rotational factor is shown in Fig. 5.

It is seen that the effect of notch sharpness on the COD from clip gage and that on the COD from S.Z. are similar, although the former is a little larger than the latter. It should be noticed that the notch tip COD at fibrous crack initiation and the stretched zone width observed on the fracture surface of the specimen will be physically the same parameters. Because, it seems to be appropriate to consider that some differences observed in Fig. 28 between the notch tip COD obtained from clip gages and $\sqrt{2} \times \text{S.Z.W.}$ come mainly

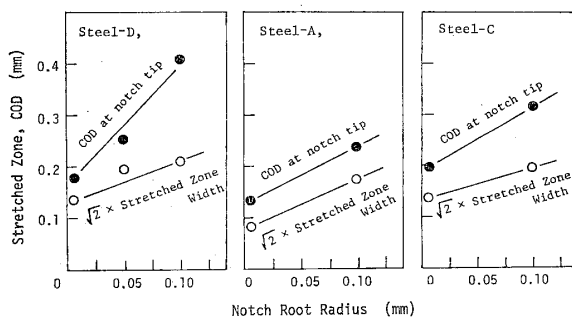


Fig. 28 The effects of notch sharpness on notch tip COD and stretched zone width

from the method to convert the measured value of COD and stretched zone width to the "crack tip displacement".

It has been pointed out by several authors and also in part I of this paper that the notch tip COD at fibrous crack initiation, δ_i , is independent of temperature⁹⁾, specimen geometry^{6,7,8)}, strain rate⁹⁾ and so on, although the COD at maximum load or unstable fracture varies largely according to the parameters cited above. Although the measurements of S.Z.W. have not been made in these experiments, the characteristics reported on δ_i seem to be the consequence of the behavior of S.Z.W. It is usual, however, that some differences between S.Z.W. and COD exist. These differences, as mentioned above, mainly come from the procedure to convert the measured COD to notch tip value.

(4) The Effects of Preloading

Before entering into the discussion on the effects of preloading on critical COD, the relation between the notch tip behavior and critical COD will be considered.

Fracture behaviors are divided into three temperature regions as already shown in Figs. 25~27. In the region 1 fracture occurs by fibrous crack, and the critical COD (measured at initial notch tip) at unstable fracture will be given by the sum of the $\sqrt{2} \times \text{S.Z.W.}$, displacement due to the opening by fibrous crack and elastic deformation as

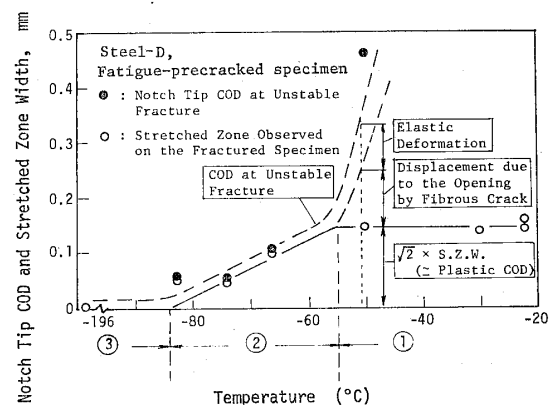


Fig. 29 Notch tip COD and stretched zone width at various temperatures

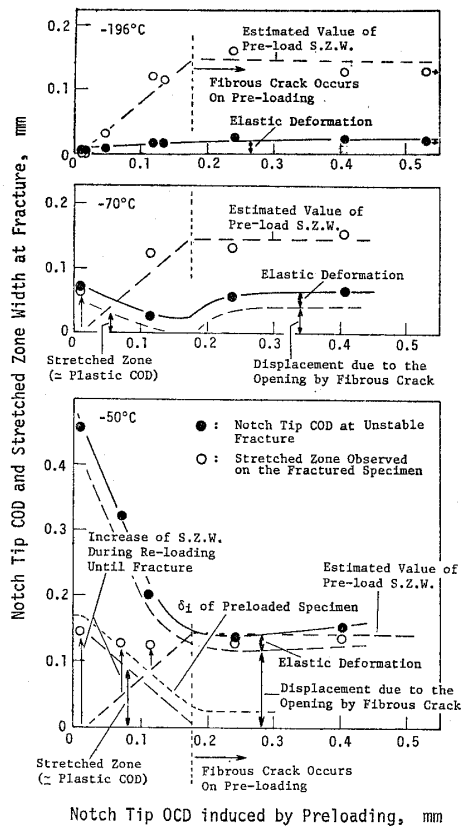


Fig. 30 Effects of preloading on notch tip COD and stretched zone width at fracture at -196°C (cleavage fracture without stretched zone), -70°C (cleavage fracture with stretched zone), and -50°C (fibrous fracture), Steel-D, fatigue-precracked specimen

shown in Fig. 29. In the region 2 fracture occurs by cleavage with stretched zone, and COD consists of $\sqrt{2} \times \text{S.Z.W.}$ and elastic deformation. In the region 3 fracture occurs by cleavage without stretched zone. In this region the critical COD mainly consists of elastic deformation.

Figure 30 shows the effects of preloading on the fracture initiation. In this figure, the critical COD at unstable fracture, stretched zone width observed on the fractured specimens and the estimated values of stretched zone width given by preloading are shown as the functions of the amount of preload COD. Preloading was given at room temperature, and the fracture tests of the preloaded specimens were made at -196°C ,

-70°C and -50°C which correspond to the temperature regions 3, 2 and 1, respectively, in Fig. 29.

In the case of the tests at -196°C , the critical COD mainly consists of elastic deformation and the effects of preloading are small.

At -70°C , in the region of smaller preload COD than that of fibrous crack initiation, the critical COD decreases with increase of the preload COD by the amount of stretched zone given by preloading. In the region of a larger preload COD than that of fibrous crack initiation, the critical COD seems to take a larger value with increase of the preload COD, probably because of the displacement due to the opening of fibrous crack.

At -50°C , in the region of a smaller preload COD than that of fibrous crack initiation, the critical COD decreases with increase of the stretched zone by the amount larger than the stretched zone width given by preloading. In the case of larger preloading than the fibrous crack initiation, the effect of preloading is almost constant regardless of the amount of preloading. It should be noticed that the stretched zone widths observed on the fracture surface (shown by open circles) show constant values regardless of the amounts of preloading. In other words, if the stretched zone induced by preloading is smaller than the stretched zone width necessary to induce fibrous fracture (S_i), the total stretched zone width (preload S.Z.W. plus increase of S.Z.W. during fracture test) is constant.

This result seems to be reasonable because fibrous crack initiation will occur when the total amount of plastic strain at the notch tip, which corresponds to total stretched zone width, reaches a critical value which will depend on the spacings of particles as suggested by Rice^{22,23}. If the preload S.Z.W. is larger than the S_i , the stretched zone width does not show any further increase in fracture tests. It should also be noticed that such special region as stretched zone was not observed between fibrous crack which occurred

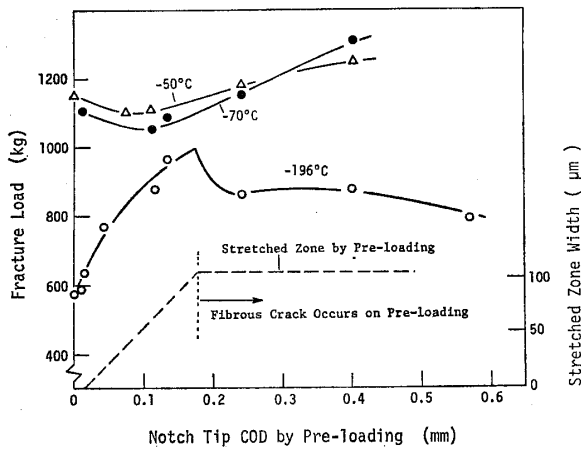


Fig. 31 Fracture loads of preloaded specimens

in preloading and which occurred in fracture tests.

The effects of preloading on the fracture load at various test temperatures are shown in Fig. 31. It is noticed that fracture load at -196°C increases with increase of the amount of preloading in the region of smaller preloading than fibrous crack initiation. In the region of larger preload than this, the

fracture load decreases with increase of preloading. The increase of fracture load in the smaller preload region will be explained by the blunting of crack tip by the formation of stretched zone, and the reduction in strength in larger preload region will be explained by the occurrence of fibrous crack at the notch root.

In the case of the tests at -50°C and -70°C , the relation between fracture load and preload is not so clear. But the strengthening in the larger preload region will be the results of work hardening which occurred during Preloading. The effects of this type seemed to occur because of the three point bend tests used in the present experiment, because in the bend tests severe plastic deformation occurs in net section of the specimens when fibrous fracture occurs. In large tensile specimens or in actual structures this type of strengthening effect by preloading would not be expected.

(5) *Stretched Zone and COD in Mixed Mode Condition*

Some examples of electron fractographs and

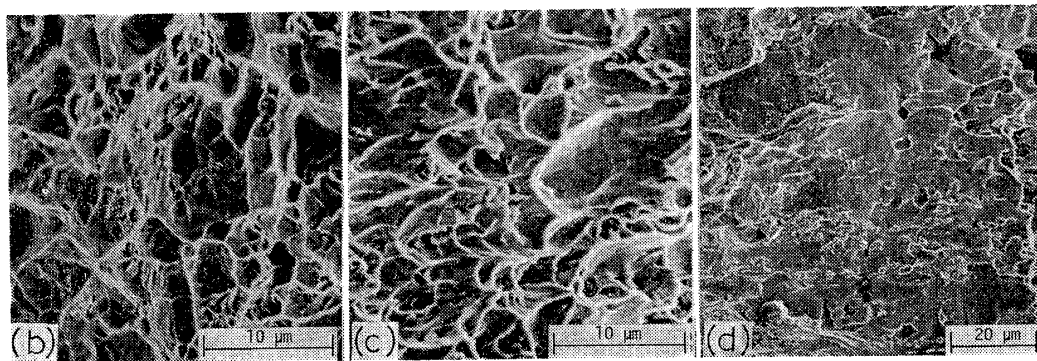
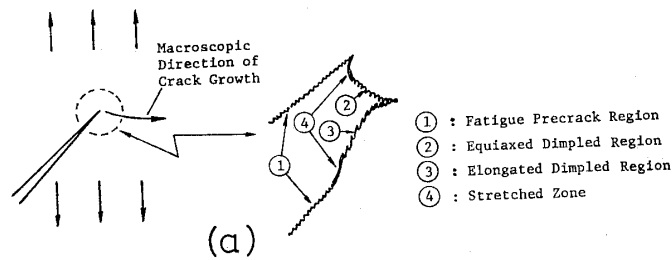


Fig. 32 Fractographs of the areas near the notch tip of the 45° fatigue-precracked specimen, Steel-E. (a) Schematic illustration of the notch tip of 45° fatigue-precracked specimen under tension, (b) Equiaxed dimples observed at ②, (c) Elongated dimples observed at ③, (d) Stretched zone observed at ④

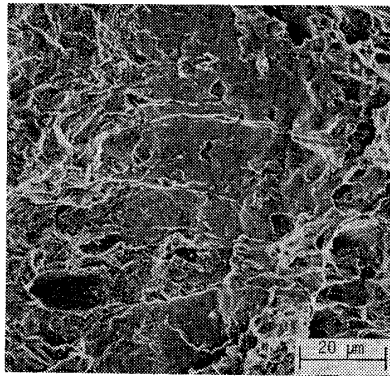


Fig. 33 Stretched zone of 90° fatigue-precracked specimen, Steel-E

schematic sketch near the notch tip of 45°-precracked specimen are shown in Figs. 32 and 33. The stretched zone width of 45°-precracked specimen is about the same as that of 90°-precracked specimen. In the case of Steel E, they are about 50~60 μm for one side of fracture surface. And it is noticed that the fracture surface of the upper side (in the figure) mainly consists of equiaxed dimples as shown in Fig. 32(b), while the mating fracture surface of the lower side consists of elongated dimples as shown in Fig. 32(c). The process of the formation of such type of fractographs in mating fracture surfaces under combined shearing-and-tearing fracture has been explained by Beachem²⁴⁾.

The appearances of the stretched zone in

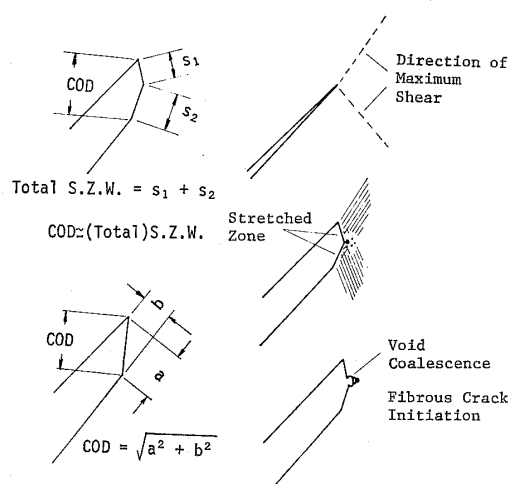


Fig. 34 Fibrous crack initiation process at the tip of 45° fatigue-precrack

45°-precracked specimens are similar to those in 90°-precracked specimens as shown in Figs. 32(d) and Fig. 33.

The process to induce fracture at the tip of 45°-precracked specimens is considered to be as shown in Fig. 34 which is essentially similar to the case of Model I specimen. The COD and the stretched zone width for oblique cracked specimen may be defined as shown in this figure. The value of COD at fibrous crack initiation defined in this way seems to be independent of slit angle.

(6) The Relation between Fracture Mechanism and Stretched Zone Width

Because the stretched zone width observed on the fracture surface corresponds to the COD at fracture initiation as discussed before, the discussion made in part I section 1.3 (3) on the relation between fracture mechanism and COD-criterion will be applicable to the results on the stretched zone width shown in Figs. 25~27. It should be noticed that the region I in Fig. 17 corresponds to region 1 in Figs. 25~27, region II and III to region 2 and region IV to region 3, respectively.

(7) Fracture Toughness Evaluation of Steel by δ_i and T_i

It is obvious that there are many cases where toughness evaluation based on fracture initiation is preferable to that based on unstable fracture. In those cases, toughness evaluation by T_i and δ_i seems to be very profitable, because δ_i seems to be a material constant as shown in section 1.3 (2) and T_i may be assumed to correspond directly to the lowest temperature at which the structure may be used, provided that the appropriate test specimens with equivalent plastic constraint to that of the actual structures could be found. δ_i will be obtained from the stretched zone width without the measurement of COD.

II.4 Conclusions

1) The stretched zone width observed on the fractured surface shows the notch tip COD at the fracture initiation.

2) In the case of fibrous crack initiation, the notch tip COD (δ_i) and S.Z.W. (S_i) are constants regardless of test temperature, specimen geometries, preloading (if the total δ_i is taken), slit angle, strain rate⁹⁾ and so on. COD will be most appropriate criterion for this case.

3) In the case of cleavage fracture initiation, stretched zone width and COD take various values between the value at the fibrous crack initiation (δ_i or S_i) and almost zero.

4) Toughness of steels, based on the fracture initiation from a precrack, will be defined by δ_i ($\approx \sqrt{2} S_i$) and T_i , where T_i is the temperature at which the transition from fibrous to cleavage initiation occurs. T_i varies largely according to the parameters cited in (2).

Acknowledgement

The authors would like to thank Mr. N. Kasai, for his assistance in experimental work.

References

- 1) T. KANAZAWA, H. MIMURA, S. MACHIDA, T. MIYATA and Y. HAGIWARA: Critical Considerations on the Criteria for Brittle Fracture Initiation, *J. Soc. Nav. Arch. Japan*, Vol. 129, pp. 237-246 (1971) (in Japanese)
- 2) F.M. BURDEKIN, and M.G. DAWES: Practical Use of Linear Elastic and Yielding Fracture Mechanics with Particular Reference to Pressure Vessels, *Practical Application of Fracture Mechanics to Pressure Vessel Technology*, Inst. Mech. Engr., pp. 28-37 (1971)
- 3) T. KANAZAWA, S. MACHIDA, T. MIYATA and Y. HAGIWARA: A Consideration of the Variables Included in the Critical COD Value in the Brittle Fracture Problem of Steel, *Proc. Inter. Conf. Mech. Behavior of Mat., Soc. Mat. Sci., Japan*, Vol. 1, pp. 493-502 (1972)
- 4) T. KANAZAWA, S. MACHIDA and Y. HAGIWARA: Study on COD Bend Test as an Engineering Brittle Fracture Initiation Characteristics Test, *J. Soc. Nav. Arch. Japan*, Vol. 132, pp. 361-370 (1972), (in Japanese)
- 5) Methods for Crack Opening Displacement (COD) Testing, DD19, British Standards Institution (1972)
- 6) P. TERRY and J.T. BARNBY: Determining Critical Crack Opening Displacement for the Onset of Slow Tearing in Steels, *Metal Const. and Brit. W.J.*, Vol. 3, pp. 343-345 (1971)
- 7) G.D. FEARNEHOUGH, G.M. LEES, J.M. LOWES and R.T. WEINER: The Role of Stable Ductile Crack Growth in the Failure of Structures, *Practical Application of Fracture Mechanics to Pressure Vessel Technology*, Inst. Mech. Engr., pp. 119-128 (1971)
- 8) R.F. SMITH and J.F. KNOTT: Crack Opening Displacement and Fibrous Fracture in Mild Steel, *Practical Application of Fracture Mechanics to Pressure Vessel Technology*, Inst. Mech. Engr., pp. 65-75 (1971)
- 9) S. KANAZAWA, K. MINAMI, K. MIYA, M. SATO and I. SOYA: An Investigation of Static COD and Dynamic COD, *J. Soc. Nav. Arch. Japan*, Vol. 133, pp. 257-265 (1973) (in Japanese)
- 10) J.M. BARSOM and S.T. ROLFE: K_{IC} Transition-Temperature Behavior of A517-F Steel, *Eng. Frac. Mech.*, Vol. 2, pp. 341-357 (1971)
- 11) G.T. HAHN, B.L. AVERBACH, W.S. OWEN and M. COHEN: Initiation of Cleavage Microcracks in Polycrystalline Iron and Steel, *Fracture*, ed. by Averbach *et al.*, MIT Press, pp. 91-116 (1959)
- 12) F.A. McCLINTOCK: On the Mechanics of Fracture from Inclusions, *Ductility*, ASM, pp. 255-277 (1968)
- 13) T. YOKOBORI: *An Interdisciplinary Approach to Fracture and Strength of Solids*, Wolters-Noordhoff (1968)
- 14) A.N. STROH: The Formation of Cracks as a Result of Plastic Flow, *Proc. Roy. Soc., Ser. A*, Vol. 223, pp. 404-414 (1954)
- 15) A.H. COTTRELL: Theory of Brittle Fracture in Steel and Similar Metals, *Trans. AIME*, Vol. 212, pp. 192-203 (1958)
- 16) C.G. CHIPPERFIELD, J.F. KNOTT and R.F. SMITH: Critical Crack Opening Displacement in Low Strength Steels. *Conf. Book of the 3rd Int. Conf. Fracture, Munich, Teil II*, I-233 (1973)
- 17) W.A. SPITZIG: A Fractographic Feature of Plane-Strain Fracture in 0.45C-Ni-Cr-Mo Steel. *Trans. ASM*, Vol. 61, pp. 344-349 (1968)
- 18) J.P. TANAKA, C.A. PAMPILLO and J.R. LOW, JR: Fractographic Analysis of the Low Energy Fracture of an Aluminum Alloy. *ASTM Spec. Tech. Publ.*, 463, pp. 191-215 (1970)

- 19) K. SCHWALBE: Processes at the Tip of a Crack Under Continuously Increasing Loads. Conf. Book of the 3rd Int. Conf. Fracture, Munich, Teil-IV, III-515 (1973)
- 20) D. ELLIOTT: Crack Tip Processes Leading to Fracture. *The Practical Implications of Fracture Mechanisms*, The Inst. of Metallurgists, pp. 21-27 (1973)
- 21) D. BROEK: Correlations between Stretched Zone Size and Fracture Toughness, *Eng. Frac. Mech.*, Vol. 6, pp. 173-181 (1974)
- 22) J.R. RICE and M.A. JOHNSON: The Role of Large Crack Tip Geometry Changes in Plane Strain Fracture, *Inelastic Behavior of Solids*, ed. by M.F. Kanninen et al., McGraw-Hill, pp. 641-672 (1970)
- 23) J.R. RICE: Crack Tip Plasticity and Fracture Initiation Criteria, Conf. Book of the 3rd Int. Conf. Fracture, Munich, Teil II, I-441 (1973)
- 24) C.D. BEACHEM and G.R. YODER: Elastic-Plastic Fracture by Homogeneous Microvoid Coalescence Tearing Along Alternating Shear Planes, *Metallurgical Transactions*, Vol. 4, pp. 1145-1153 (1973)